

High Mobility Surface InAs Two-dimensional Heterostructures for Hybrid Superconductor-Semiconductor Systems

Kaushini S. Wickramasinghe^{1,2}, William Mayer¹, Joseph Yuan¹,
Tri Nguyen³, Vladimir Manucharyan², and Javad Shabani¹

¹*Center for Quantum Phenomena, Department of Physics, New York University, NY 10003, USA*

²*Department of Physics, University of Maryland, College Park, MD 20742, USA*

³*Department of Physics, City College of City University of New York, New York City, NY 10031, USA*

(Dated: July 4, 2022)

Two dimensional electron systems (2DES) confined to the surface of narrowband semiconductors have attracted great interest since they can easily integrate with superconductivity (or ferromagnetism) enabling new possibilities to engineer topological states in solid state systems. In this work, we study indium arsenide (InAs) heterostructures where combining superconductivity, low density, and spin-orbit coupling can be achieved. We study the magnetotransport as a function of top barrier and density and report clear observation of integer quantum Hall states. Spin orbit interaction parameters, deduced from weak-antilocalization, can be tuned over large density range ($\sim 10^{12} \text{ cm}^{-2}$). We model various scattering mechanisms and find out un-doped optimal structure can improve electron mobility to exceed $44,000 \text{ cm}^2/\text{Vs}$.

Epitaxial two-dimensional heterostructures containing InAs layers are hypothesized to be a suitable system for spintronics applications¹. Spintronics favors materials like InAs with strong spin orbit interaction (SOC) and large g-factor. Recently, two-dimensional electron systems (2DESS) confined to surface InAs layers have become the focus of renewed theoretical and experimental attention partly because of their potential applications in topological² and superconducting quantum computation^{3–5}. However, all these applications require precise control of electrostatic potentials and carrier densities using nano-fabricated metallic gates. Unlike ubiquitous Gallium Arsenide (GaAs) based systems, reliable gating has proven challenging in InAs based systems due to gate leakage and hysteretic behavior. Charge traps and surface Fermi level pinning can drastically affect device performance. Some of these challenges have been solved using surface passivation⁶ or different top layers⁷, however, new applications require epitaxial contacts to metals and hence require quantum wells that are positioned at the surface⁸. Furthermore the proximity of the contact has to be tuneable for each application. In some cases high mobility⁹ and in other cases control over the induced gap is desired¹⁰.

In recent years engineering novel quasiparticles, Majorana zero modes, in semiconductors with strong SOC (InAs, InSb) in proximity of conventional superconductors (Al, Nb)^{11–14} has only intensified. In order to probe and establish their statistics and eventually move beyond demonstrations of zero bias signatures to braiding^{15,16} and larger-scale Majorana networks^{17,18}, it is likely that a top-down patterning approach will be needed. Growth of large-area 2D Superconductor-Semiconductor systems through Molecular Beam Epitaxy (MBE) can provide the basis for such an approach. Josephson Junctions have been studied⁸ and signatures of Majorana fermions have been explored^{19,20} on such 2D hybrid InAs-Al platforms. The question remains how well one can control the 2DES at the surface. For example, if such 2DEGs

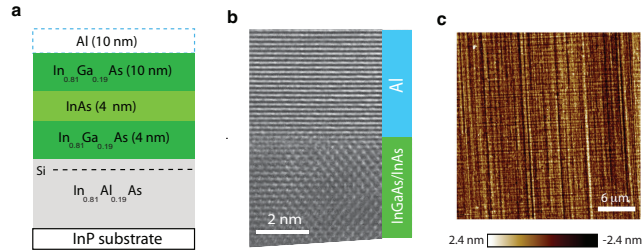


FIG. 1: (Color online) (a) General structure of hybrid Al-InAs surface quantum well. (b) High-resolution transmission microscope image showing that the Al forms a sharp and uniform interface to the InGaAs layer. (c) Atomic force microscopy image shows the surface roughness of about 0.8 nm.

exhibit integer and fractional quantum Hall states one might be able to engineer a system to host parafermion quasiparticle^{21,22}. In this work, we carefully study the electronic transport of these surface InAs structures. We show we can achieve InAs/InGaAs structures with mobilities reaching near $44,000 \text{ cm}^2/\text{Vs}$ and clear observation of integer quantum Hall states. The optimized structure provides a semiconducting platform with lower disorder and higher mobility than previously reported^{8,23}.

The samples were grown on semi-insulating InP (100) substrates in a modified Gen II MBE system. The step graded buffer layer, $\text{In}_x \text{Al}_{1-x} \text{As}$, is grown at low temperature to minimize dislocations forming due to the lattice mismatch between the active region and the InP substrate^{7,24,25}. The quantum well consists of a 4 nm layer of InAs grown on a 4 (or 6) nm layer $\text{In}_{0.81} \text{Ga}_{0.19} \text{As}$. A top layer, typically 10 nm of $\text{In}_{0.81} \text{Ga}_{0.19} \text{As}$, is grown on InAs strained quantum well as shown in Fig. 1a. After the quantum well is grown, the substrate is cooled to promote the growth of epitaxial Al (111)⁸. Figure 1b shows a high-resolution transmission electron microscope (TEM) image of this interface between Al and $\text{In}_{0.81} \text{Ga}_{0.19} \text{As}$, with atomic planes of both crystals clearly visible. All

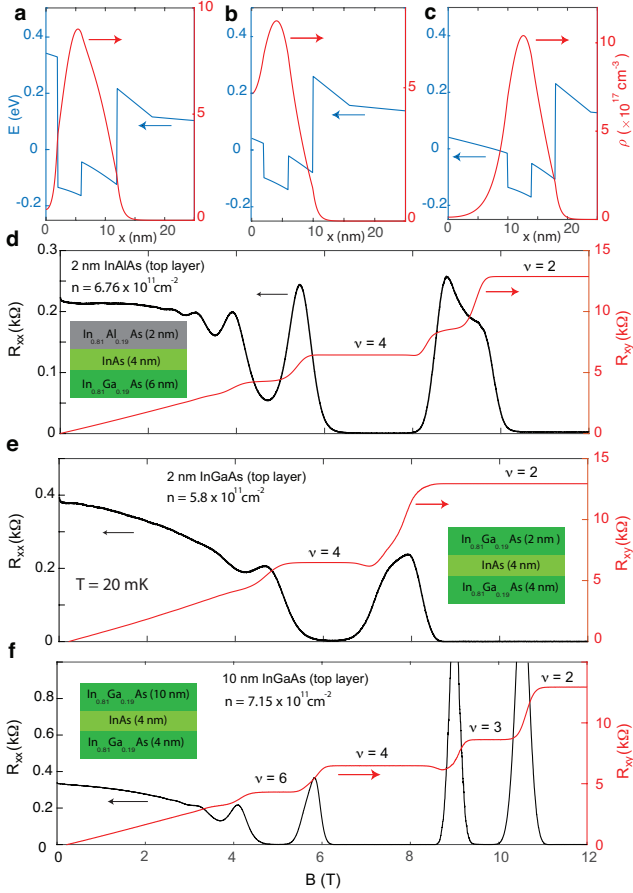


FIG. 2: (Color online) Self consistent Poisson charge distribution calculations for top layers of (a) 2 nm InAlAs, (b) 2 nm InGaAs, and (c) 10 nm InGaAs. Magnetotransport and layer structure of InAs quantum wells with top layers of (d) 2 nm InAlAs, (e) 2 nm InGaAs, and (f) 10 nm InGaAs.

samples reported in this paper have had Al thin films grown and thin films of Al were selectively removed for transport studies of the InAs quantum well. The surface roughness of samples do not change with or without Al thin films confirmed by atomic force microscope images. Figure 1c shows a surface topography of a sample with InGaAs top layer on a $34 \mu\text{m}$ by $34 \mu\text{m}$ square.

The Fermi level pinning at semiconductor surfaces has been the subject of numerous theoretical and experimental studies. In most semiconductors, such as GaAs, the Fermi level is pinned inside the band gap²⁶. It is well known that the surface states in case of InAs can result in a two dimensional electron system²⁷. The electron accumulation is due to pinning of the Fermi level above the conduction band minimum. The position of the pinning level depends on the material and the surface treatments⁶. Experiments on $\text{In}_x\text{Ga}_{1-x}\text{As}$ predicts Schottky barrier height becomes negative, exhibiting an ohmic behavior, for $x > 0.85$ ²⁸. Low temperature transport properties of surface accumulation InAs structures are dominated by surface scattering (low mobility,

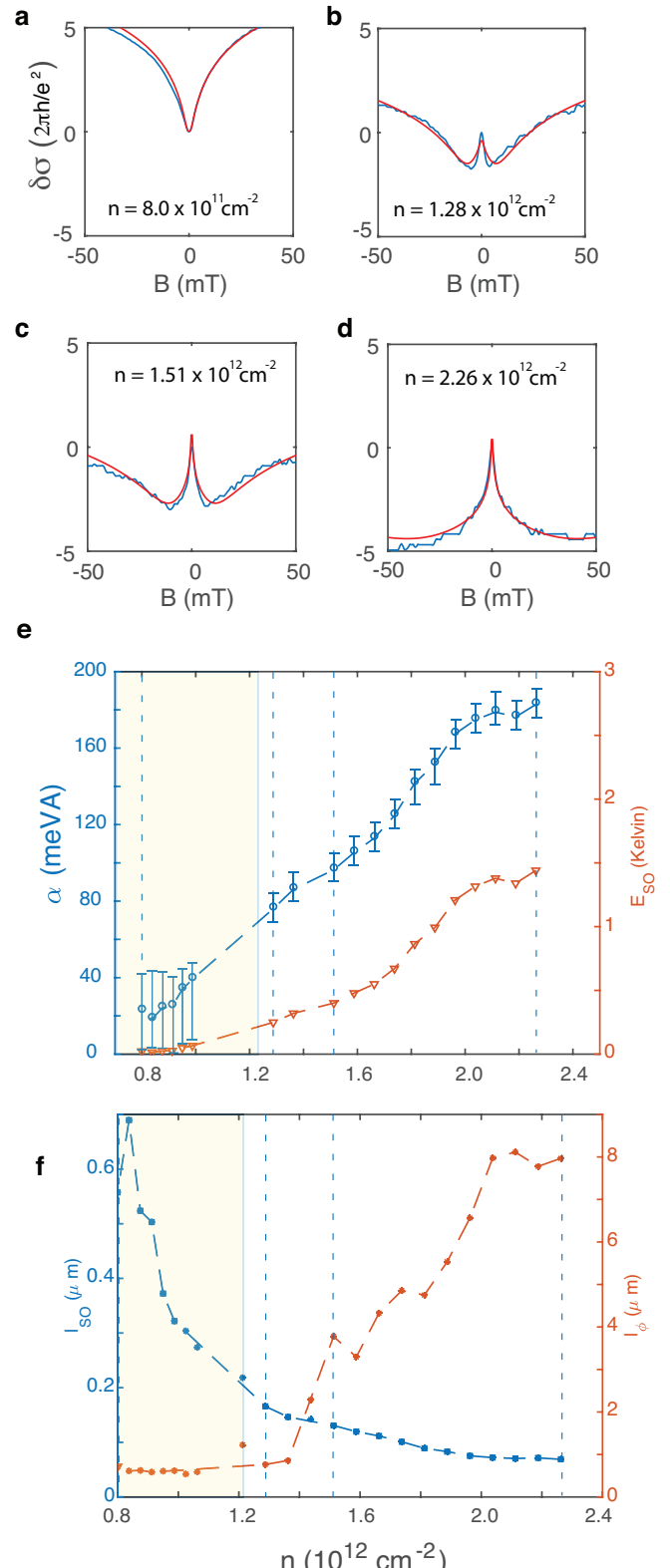


FIG. 3: (Color online) Low magnetic field response of InAs 2DES for densities: (a) $n = 8.0 \times 10^{11} \text{ cm}^{-2}$ (b) $1.28 \times 10^{12} \text{ cm}^{-2}$ (c) $1.51 \times 10^{12} \text{ cm}^{-2}$ (d) $2.26 \times 10^{12} \text{ cm}^{-2}$. The fit using ILP model is shown in red, see text. (e) Rashba SOC parameter, α (left axis) and corresponding spin orbit gap E_{SO} (right axis) as a function of density. (f) Spin orbit length (left axis) and phase coherence length (right axis) as a function of density. Dashed lines corresponds to densities in part (a-d). Shaded regions in parts (e) and (f) denote $l_{SO} \geq l_\phi$ where the fits are no longer valid for extracting spin orbit parameters.

limited to a 1000-3000 cm²/Vs) and magnetotransport shows very weak signatures of Shubnikov-de Haas oscillations. Adding a top layer to pure InAs quantum well resolves these issues. One natural choice is using InAlAs as the top layer. InAlAs has a large electron mass and forms a ~ 400 meV barrier next to InAs. Self-consistent Poisson-Schrodinger calculation shows the charge distribution vanishes by 5 nm of In_{0.81}Al_{0.19}As. We have studied samples with 2 and 5 nm of InAlAs top layers. Figure 2d shows the longitudinal and Hall resistance traces of a van der Pauw sample with 2 nm InAlAs top layer. The corresponding charge distribution is also shown in Fig. 2a. The second option is to use InGaAs which has a similar effective electron mass to InAs and the resulting hybrid quantum well structure supports confinement of the wave function both in InGaAs and InAs layers^{8,29}. Figure 2e shows the magnetotransport data of a sample with 2 nm InGaAs top layer. As evidenced by charge distribution calculations in Fig. 2b, there is a strong overlap with the surface. However the electron mobility and visibility of quantum Hall states are reduced. The onset of oscillations for the InAlAs 2 nm top layer sample is near 2 T ($\mu = 8,500$ cm²/Vs) and for the 2 nm InGaAs top layer sample is near 3 T ($\mu = 6,500$ cm²/Vs). All measurements are performed at 20 mK.

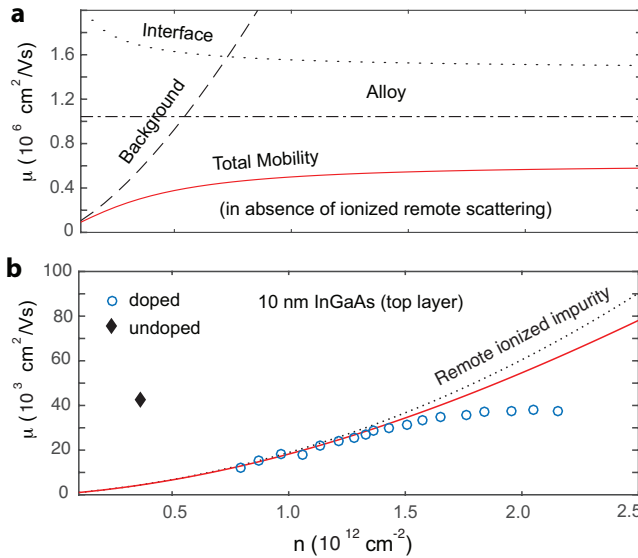


FIG. 4: (Color online) (a) Calculated mobilities from different scattering mechanisms as a function of doping electron density for buried quantum wells. (b) Total theoretical mobility versus measured mobility for surface quantum wells.

Engineering the coupling of the 2DEG with surface is an important knob in tuning the proximity effect in Josephson devices. The goal is to keep the finite charge distribution at the surface *in addition to* highest electron mobility and quality of magnetotransport. We have studied several samples with various InGaAs top layer thicknesses and have found that a 10 nm top layer thickness yields the highest quality 2DEG as well as good

wavefunction overlap at the surface³⁰. The magnetotransport shown in Fig. 2f (with corresponding charge distribution in Fig. 2c). While electron density has not changed much, the quality has increased with onset of oscillations at 2.25 T and $\mu = 14,400$ cm²/Vs. We also observe a well developed $\nu = 3$ and 6 which were not present in thinner top layers. Recent studies show that having a strong spin-orbit coupling may be compromised in strongly coupled limit, and somewhat weaker interface tunneling may be necessary for achieving optimal proximity¹⁰ and estimated to be 10 nm in case of In_{0.81}Ga_{0.19}As⁸. For the rest of this paper we focus on properties of structures with 10 nm thick In_{0.81}Ga_{0.19}As top layer.

We next analyze the spin orbit coupling using low field weak antilocalization measurements. These measurements are performed on gated Hall bars fabricated using optical photolithography and wet etch techniques. A standard low-frequency lock-in technique with an excitation current of 10 nA to 100 nA was used to measure the signal as a function of a perpendicular magnetic field. Fig. 3(a-d) show the measured corrections to conductivity as a function of density (data in blue). At $n = 8.0 \times 10^{11}$ cm⁻², the valley in conductivity shows absence of strong Rashba coupling while with increasing density a peak appears and develops into a strong peak with increasing density to highest density we probe $n = 2.26 \times 10^{12}$ cm⁻². The data is analyzed using the theory developed by Iordanskii, Lyanda-Geller, and Pikus (ILP) for two-dimensional electron systems (2DESs)³¹. To reduce the number of free fitting parameters we fixed the value of cubic Dresselhaus SOC, γ as the bulk value of InAs 26.9 eV Å³ calculated from the $\vec{k} \cdot \vec{p}$ theory³². Fitting $\delta\sigma(B)$ over the range $|B| < 50$ mT at T = 20 mK yields the linear spin-orbit coupling parameter, α shown in Fig. 3e, and phase-coherence length, l_ϕ shown in Fig. 3f. At high densities, Rashba SOC parameter reaches about 200 meVÅ and spin orbit energy gap, E_{SO} reaches 1.5 K. Similarly, l_ϕ reaches to about 8 μm and l_{SO} to 100 nm with a ratio of $l_\phi/l_{SO} \sim 80$.

The density dependence of the electron mobility can illuminate the various sources contributing to scattering. Fig. 4a shows calculated mobility due to scattering from rough interface, alloy scattering and background doping which are all relevant for deep structures (100 to 200 nm of InAlAs top layer)^{7,25}. The alloy scattering is highly sensitive to the ternary composition, $\mu \sim \frac{1}{x(1-x)}$, is calculated following Ref.³³. The background doping, N_B , is deduced based on the observation that undoped deep structures conduct with density range in few 10^{11} cm⁻². Based on series of comparison between calculation and measurements we estimate $N_B \sim 10^{16}$ cm⁻³. The interface roughness with fluctuation height 0.8 nm adds a cut-off at 1.5×10^6 cm²/Vs. Based on these values, the total mobility is calculated based on the Matthiessen's rule as shown in red in Fig. 4a. For deep structures, mobility is expected to increase with electron density and saturates around 600,000 cm²/Vs similar to earlier studies⁷.

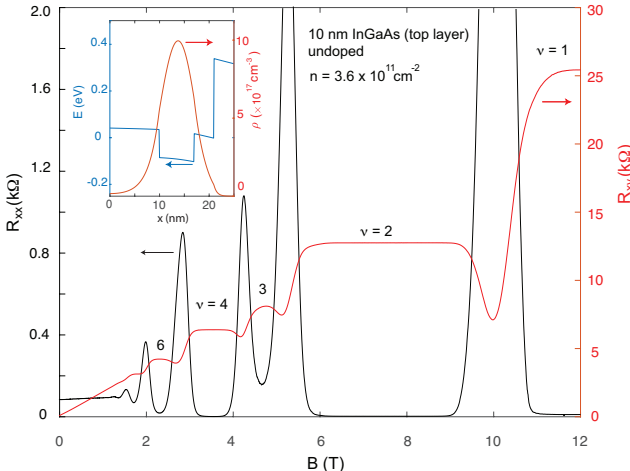


FIG. 5: (Color online) Magnetotransport for an undoped sample in the van der Pauw geometry with top layer of 10 nm $\text{In}_{0.81}\text{Ga}_{0.19}\text{As}$.

For surface quantum wells, the situation is different where surface scattering and remote ionized doping, N_d , play major roles. The dependence of the mobility on density of our sample is shown in Fig. 4b. The electron mobility varies between $10,000 \text{ cm}^2/\text{Vs}$ and $40,000 \text{ cm}^2/\text{Vs}$. The mobility starts to saturate near $1.6 \times 10^{12} \text{ cm}^{-2}$ close to second subband occupation. The data can be fitted by $\mu \sim n^\alpha$, with $\alpha = 0.9$ in density range below $1.6 \times 10^{12} \text{ cm}^{-2}$. Since the contribution of background doping is low in surface quantum wells and exact details of surface impurity scatterings are unknown, we have fitted the data with remote impurity doping³⁴ (only the lowest subband is included in the calculation) and found an upper bound $N_d \sim 10^{12} \text{ cm}^{-2}$ with which the data can be reasonably fit (red curve in Fig. 4b). Our surface quantum wells are typically doped by $\sim 10^{12} \text{ cm}^{-2}$ from the back side of the quantum well. Based on these results we studied a van der Pauw sample without back side doping. Figure 5 shows the longitudinal and Hall data at $T = 20 \text{ mK}$. As expected the electron density is reduced to $n = 3.6 \times 10^{11} \text{ cm}^{-2}$ but electron mobility is enhanced to $44,000 \text{ cm}^2/\text{Vs}$. Various integer quantum Hall states are clearly resolved at $\nu = 1, 2, 3, 4, 6, 8$ with onset of oscillation at 1.2 T . We should note that our undoped structures initially did not conduct probably due

to surface compensation. Originally during the growth, we would change the indium and aluminum cell temperatures to change the composition during step graded buffer. In all the structures we have presented in this paper, we have kept the Al cell temperature fixed while indium cell temperature has been adjusted during step graded buffer. We found that the optimum arsenic flux and growth temperatures are different and it is only in these structures that undoped surface quantum wells are conducting. The self consistent calculations estimates a carrier density of $\sim 3.3 \times 10^{11} \text{ cm}^{-2}$ assuming all charges are originating from background doping in the barriers

TABLE I: Summary of InAs surface quantum wells and their transport properties. Top layer material with indium composition of 0.81, barrier thickness in nm: d, Si doping (cm^{-2}): N_d , Electron density (cm^{-2}): n, Mobility: μ , Onset of Shubnikov-de Haas (Tesla): B_{on} .

Barrier	d	$N_d (\text{cm}^{-2})$	$n (10^{11} \text{ cm}^{-2})$	$\mu (\text{cm}^2/\text{Vs})$	$B_{on} (\text{T})$
InAlAs	5	10^{12}	10	14,000	1.5
InAlAs	2	10^{12}	6.76	8,500	2
InGaAs	2	10^{12}	5.8	6,500	3
InGaAs	10	10^{12}	7.15	14,400*	2.25
InGaAs	10	-	3.6	44,000	1.2
InGaAs	20	10^{12}	10	12,570	1.3

as shown in the inset of Fig. 5. This suggests that in optimized structures the compensation is minimal and most of carriers are coming from the barrier and without ionized impurities nearby we can improve the mobility. Table I summarizes transport properties of our InAs surface quantum wells.

In summary, we present InAs quantum wells near the surface where we can control the overlap with the surface. Having both a 2DEG at the surface and high mobility is a challenging task that can only be overcome by optimization of the structures (such as roughness, background doping) and understanding scattering mechanisms as a function of density. In addition, we can tune the Rashba spin orbit coupling using electric gate in these structures.

Our work was supported by US Army research office and DARPA.

¹ Igor Žutić, Jaroslav Fabian, and S. Das Sarma. Spintronics: Fundamentals and applications. *Rev. Mod. Phys.*, 76: 323–410, Apr 2004. doi: 10.1103/RevModPhys.76.323. URL <https://link.aps.org/doi/10.1103/RevModPhys.76.323>.

² Jason Alicea. New directions in the pursuit of majorana fermions in solid state systems. *Reports on Progress in Physics*, 75(7):076501, 2012. URL <http://stacks.iop.org/0034-4885/75/i=7/a=076501>.

³ Z. Qi, H. Xie, J. Shabani, V. E. Manucharyan, A. Levchenko, and M. G. Vavilov. Controlled-z gate for transmon qubits coupled by semiconductor junctions. *arXiv:1801.04291*.

⁴ L. Casparis, M. R. Connolly, M. Kjaergaard, N. J. Pearson, A. Kringhoj, T. W. Larsen, F. Kuemmeth, T. Wang, C. Thomas, S. Gronin, G. C. Gardner, M. J. Manfra, C. M. Marcus, and K. D. Petersson. Superconducting gatemon qubit based on a proximitized two-dimensional electron

gas. *arXiv:1711.07665*.

⁵ T. W. Larsen, K. D. Petersson, F. Kuemmeth, T. S. Jespersen, P. Krogstrup, J. Nygård, and C. M. Marcus. Semiconductor-nanowire-based superconducting qubit. *Phys. Rev. Lett.*, 115:127001, Sep 2015. doi: 10.1103/PhysRevLett.115.127001. URL <https://link.aps.org/doi/10.1103/PhysRevLett.115.127001>.

⁶ L. Canali, J.W.G. Wildoer, O. Kerkhof, and L.P. Kouwenhoven. Low-temperature stm on inas(110) accumulation surfaces. *Appl Phys A*, 66:113, 1998.

⁷ J. Shabani, A. P. McFadden, B. Shojaei, and C. J. Palmstrøm. Gating of high-mobility inas metamorphic heterostructures. *Applied Physics Letters*, 105(26), 2014.

⁸ J. Shabani, M. Kjaergaard, H. J. Suominen, Younghyun Kim, F. Nichele, K. Pakrouski, T. Stankevic, R. M. Lutchyn, P. Krogstrup, R. Feidenhans'l, S. Kraemer, C. Nayak, M. Troyer, C. M. Marcus, and C. J. Palmstrøm. Two-dimensional epitaxial superconductor-semiconductor heterostructures: A platform for topological superconducting networks. *Phys. Rev. B*, 93:155402, 2016.

⁹ Jay D. Sau, Sumanta Tewari, and S. Das Sarma. Experimental and materials considerations for the topological superconducting state in electron- and hole-doped semiconductors: Searching for non-abelian majorana modes in 1d nanowires and 2d heterostructures. *Phys. Rev. B*, 85:064512, Feb 2012. doi: 10.1103/PhysRevB.85.064512. URL <https://link.aps.org/doi/10.1103/PhysRevB.85.064512>.

¹⁰ William S. Cole, S. Das Sarma, and Tudor D. Stănescu. Effects of large induced superconducting gap on semiconductor majorana nanowires. *Phys. Rev. B*, 92:174511, Nov 2015. doi: 10.1103/PhysRevB.92.174511. URL <https://link.aps.org/doi/10.1103/PhysRevB.92.174511>.

¹¹ V. Mourik, K. Zuo, S. M. Frolov, S. R. Plissard, E. P. A. M. Bakkers, and L. P. Kouwenhoven. Signatures of Majorana Fermions in Hybrid Superconductor-Semiconductor Nanowire Devices. *Science*, 336:1003–, May 2012. doi: 10.1126/science.1222360.

¹² Anindya Das, Yuval Ronen, Yonatan Most, Yuval Oreg, Moty Heiblum, and Hadas Shtrikman. Zero-bias peaks and splitting in an al-inas nanowire topological superconductor as a signature of majorana fermions. *Nature Physics*, 8: 887 EP –, 11 2012. URL <http://dx.doi.org/10.1038/nphys2479>.

¹³ M. T. Deng, S. Vaitiekėnas, E. B. Hansen, J. Danon, M. Leijnse, K. Flensberg, J. Nygård, P. Krogstrup, and C. M. Marcus. Majorana bound state in a coupled quantum-dot hybrid-nanowire system. *Science*, 354 (6319):1557–1562, 2016. ISSN 0036-8075. doi: 10.1126/science.aaf3961. URL <http://science.scienmag.org/content/354/6319/1557>.

¹⁴ Önder Güç, Hao Zhang, Jouri D. S. Bommer, Michiel W. A. de Moor, Diana Car, Sébastien R. Plissard, Erik P. A. M. Bakkers, Attila Geresdi, Kenji Watanabe, Takashi Taniguchi, and Leo P. Kouwenhoven. Ballistic majorana nanowire devices. *Nature Nanotechnology*, 2018. doi: 10.1038/s41565-017-0032-8. URL <https://doi.org/10.1038/s41565-017-0032-8>.

¹⁵ Jason Alicea, Yuval Oreg, Gil Refael, Felix von Oppen, and Matthew P. A. Fisher. Non-abelian statistics and topological quantum information processing in 1d wire networks. *Nat Phys*, 7(5):412–417, 05 2011. URL <http://dx.doi.org/10.1038/nphys1915>.

¹⁶ Bertrand I. Halperin, Yuval Oreg, Ady Stern, Gil Refael, Jason Alicea, and Felix von Oppen. Adiabatic manipulations of majorana fermions in a three-dimensional network of quantum wires. *Phys. Rev. B*, 85:144501, Apr 2012. doi: 10.1103/PhysRevB.85.144501. URL <http://link.aps.org/doi/10.1103/PhysRevB.85.144501>.

¹⁷ Jason Alicea, Yuval Oreg, Gil Refael, Felix von Oppen, and Matthew P. A. Fisher. Non-abelian statistics and topological quantum information processing in 1d wire networks. *Nature Phys.*, 7(5):412–417, 05 2011. doi: 10.1038/nphys1915.

¹⁸ Alex Matos-Abiague, Javad Shabani, Andrew D. Kent, Geoffrey L. Fatin, Benedikt Scharf, and Igor Zutic. Tunable magnetic textures: From majorana bound states to braiding. *Solid State Communications*, 262:1 – 6, 2017. ISSN 0038-1098. doi: <https://doi.org/10.1016/j.ssc.2017.06.003>. URL <http://www.sciencedirect.com/science/article/pii/S0038109817301904>.

¹⁹ H. J. Suominen, M. Kjaergaard, A. R. Hamilton, J. Shabani, C. J. Palmstrøm, C. M. Marcus, and F. Nichele. Zero-energy modes from coalescing andreev states in a two-dimensional semiconductor-superconductor hybrid platform. *Phys. Rev. Lett.*, 119:176805, Oct 2017. doi: 10.1103/PhysRevLett.119.176805. URL <https://link.aps.org/doi/10.1103/PhysRevLett.119.176805>.

²⁰ Fabrizio Nichele, Asbjørn C. C. Drachmann, Alexander M. Whiticar, Eoin C. T. O'Farrell, Henri J. Suominen, Antonio Fornieri, Tian Wang, Geoffrey C. Gardner, Candice Thomas, Anthony T. Hatke, Peter Krogstrup, Michael J. Manfra, Karsten Flensberg, and Charles M. Marcus. Scaling of majorana zero-bias conductance peaks. *Phys. Rev. Lett.*, 119:136803, Sep 2017. doi: 10.1103/PhysRevLett.119.136803. URL <https://link.aps.org/doi/10.1103/PhysRevLett.119.136803>.

²¹ Roger S. K. Mong, David J. Clarke, Jason Alicea, Natan H. Lindner, Paul Fendley, Chetan Nayak, Yuval Oreg, Ady Stern, Erez Berg, Kirill Shtengel, and Matthew P. A. Fisher. Universal topological quantum computation from a superconductor-abelian quantum hall heterostructure. *Phys. Rev. X*, 4:011036, Mar 2014. doi: 10.1103/PhysRevX.4.011036. URL <https://link.aps.org/doi/10.1103/PhysRevX.4.011036>.

²² David J. Clarke, Jason Alicea, and Kirill Shtengel. Exotic non-abelian anyons from conventional fractional quantum hall states. *Nature Communications*, 4:1348 EP –, 01 2013. URL <http://dx.doi.org/10.1038/ncomms2340>.

²³ M. Kjaergaard, H. J. Suominen, M. P. Nowak, A. R. Akhmerov, J. Shabani, C. J. Palmstrøm, F. Nichele, and C. M. Marcus. Transparent semiconductor-superconductor interface and induced gap in an epitaxial heterostructure josephson junction. *Phys. Rev. Applied*, 7: 034029, Mar 2017. doi: 10.1103/PhysRevApplied.7.034029. URL <https://link.aps.org/doi/10.1103/PhysRevApplied.7.034029>.

²⁴ X. Wallart, J. Lastennet, D. Vignaud, and F. Mollot. Performances and limitations of inasinalas metamorphic heterostructures on inp for high mobility devices. *Appl. Phys. Lett.*, 87:043504, 2005.

²⁵ J. Shabani, S. Das Sarma, and C. J. Palmstrøm. An apparent metal-insulator transition in high-mobility two-dimensional inas heterostructures. *Phys. Rev. B*, 90: 161303, Oct 2014.

²⁶ C. A. Mead and W. G. Spitzer. Fermi level position at metal-semiconductor interfaces. *Phys. Rev.*, 134:A713–A716, May 1964. doi: 10.1103/PhysRev.134.A713. URL <http://link.aps.org/doi/10.1103/PhysRev.134.A713>.

<https://link.aps.org/doi/10.1103/PhysRev.134.A713>.

²⁷ D. C. Tsui. Observation of surface bound state and two-dimensional energy band by electron tunneling. *Phys. Rev. Lett.*, 24:303–306, Feb 1970. doi: 10.1103/PhysRevLett.24.303. URL <https://link.aps.org/doi/10.1103/PhysRevLett.24.303>.

²⁸ K. Kajiyama, Y. Mizushima, and S. Sakata. Schottky barrier height of nInGaAs diodes. *Appl. Phys. Lett.*, 23:458, 1973.

²⁹ M. Kjaergaard, H. J. Suominen, M. P. Nowak, A. R. Akhmerov, J. Shabani, C. J. Palmstrøm, F. Nichele, and C. M. Marcus. Transparent semiconductor-superconductor interface and induced gap in an epitaxial heterostructure josephson junction. *Phys. Rev. Applied*, 7: 034029, Mar 2017. doi: 10.1103/PhysRevApplied.7.034029. URL <https://link.aps.org/doi/10.1103/PhysRevApplied.7.034029>.

³⁰ Josephson devices fabricated on these structures with 10 nm InGaAs top layer thickness exhibit $I_C R_N \sim 200 \mu V$.

³¹ S. V. Iordanskii, Y. B. Lyanda-Geller, and G. E. Pikus. *JETP Lett.*, 60:206, 1994.

³² W. Knap, C. Skierbiszewski, A. Zduniak, E. Litwin-Staszewska, D. Bertho, F. Kobbi, J. L. Robert, G. E. Pikus, F. G. Pikus, S. V. Iordanskii, V. Mosser, K. Zekentes, and Yu. B. Lyanda-Geller. Weak antilocalization and spin precession in quantum wells. *Phys. Rev. B*, 53:3912–3924, 1996.

³³ D. Chattopadhyay. Alloy scattering in quantum-well structures of semiconductor ternaries. *Phys. Rev. B*, 31:1145–1146, Jan 1985. doi: 10.1103/PhysRevB.31.1145. URL <https://link.aps.org/doi/10.1103/PhysRevB.31.1145>.

³⁴ A. Gold. Electronic transport properties of a two-dimensional electron gas in a silicon quantum-well structure at low temperature. *Phys. Rev. B*, 35:723–733, Jan 1987. doi: 10.1103/PhysRevB.35.723. URL <https://link.aps.org/doi/10.1103/PhysRevB.35.723>.